Cocrystal habit engineering to improve drug dissolution and alter derived powder properties

Dolores. R. Serrano[1], Peter. O'Connell[1], Krzysztof J. Paluch[2], David Walsh[1], Anne Marie Healy[1,*]

[1] School of Pharmacy and Pharmaceutical Sciences, Trinity College Dublin, Dublin 2, Ireland.

[2]School of Pharmacy, University of Bradford, Bradford, West Yorkshire, United Kingdom.

*Corresponding author:

Tel.: +353 1 896 1444; fax: +353 1 896 2810.

E-mail address: healyam@tcd.ie (A.M. Healy)

Abstract

Objectives: Cocrystallization of sulfadimidine (SDM) with suitable coformers, such as 4-aminosalicylic acid (4-ASA), combined with changes in the crystal habit can favourably alter its physicochemical properties. The aim of this work was to engineer SDM:4-ASA cocrystals with different habits in order to investigate the effect on dissolution, and the derived powder properties of flow and compaction.

Methods: Cocrystals were prepared in a 1:1 molar ratio by solvent evaporation using ethanol (habit I) or acetone (habit II), solvent evaporation followed by grinding (habit III) and spray-drying (habit IV).

Key findings: Powder X-ray diffraction showed Bragg peak position was the same in all the solid products. The peak intensity varied, indicating different preferred crystal orientation confirmed by SEM micrographs: large prismatic crystals (habit I), large plate-like crystals (habit II), small cube-like crystals (habit III) and microspheres (habit IV). The habit III exhibited the fasted dissolution rate; however, it underwent a polymorphic transition during dissolution. Habits I and IV exhibited the highest Carr's compressibility index, indicating poor flowability. However, habits II and III demonstrated improved flow. Spray drying resulted in cocrystals with improved compaction properties.

Conclusions: Even for cocrystals with poor pharmaceutical characteristics, a habit can be engineered to alter the dissolution, flowability and compaction behavior.

Keywords

Cocrystal, crystal habit, dissolution, flowability, tabletability, wettability

1. Introduction

The productivity of the pharmaceutical industry is witnessing an oncoming crisis due to the increasing costs for R&D, increasingly demanding regulatory requirements imposed by both the EMA (European Medicines Agency) and FDA (Food and Drug Administration) and the physicochemical properties of drug candidates in the pipeline, characterised by very poor aqueous solubility [1,2]. Inexpensive pharmaceutical strategies are required to make high pharma quality affordable. Salt formation is a common approach to enhance drug solubility but it is not successful when the active pharmaceutical ingredient (API) does not contain ionisable functional groups in its chemical structure. Engineering of pharmaceutical cocrystals can be an advantageous strategy to overcome the issue of poor solubility, without the need to break or create covalent bonds. Hydrogen bonds are formed between the API and the coformer (one or more) which is usually a GRAS (generally regarded as safe) molecule with higher aqueous solubility[3,4]. In an ideal scenario, the API is transformed into a solid form that combines improved dissolution, that may be comparable to that obtained with the amorphous drug, with greater physical and chemical stability due to its crystalline structure[5,6]. However, two other factors "polymorphism" and "crystal habit" play a key role in the physicochemical properties of the API and then in its overall biopharmaceutical performance *in vivo*. Polymorphism is the ability of a drug to pack into different crystal lattice arrangements whereas, crystal habit is the external appearance of the crystal[7,8].

Common approaches to produce cocrystals in the pharmaceutical industry are grinding and crystallisation methods. Spray drying, a well-established scale-up technique, has also been shown to be a successful strategy to obtain pure cocrystals[9,10]. During the manufacturing process, a number of different variables such as solvent, degree of supersaturation, temperature, stirring rate, presence of other excipients, milling time and speed can affect both polymorphism and the growth of crystal facets and therefore the crystal habit[11,12]. At the same time, the resulting polymorphic form and crystal habit can affect not only the dissolution profile of the API but also the flow properties and the tableting-behaviour of the material[13]. In order to keep solid dosage form production as economical as possible, directly compressible powder is preferred over granulation, as the latter is more time and energy consuming and exposes the formulation to solvent or water and heat[13]. Even for isomorphic drugs with poor compaction behaviour and tendency to stick to the punches, a crystal habit could be engineered which results in a drug formulation with better dissolution, flowability and tableting behavior.

SDM is a poorly-soluble anti-infective agent. In spite of the increasing antibiotic resistance, sulfonamides still enjoy relatively widespread use, especially in developing countries due to their low cost and wide antibacterial spectrum[14]. Sulfonamides commonly contain multiple hydrogen bond acceptor and donor functional groups that allows multiple supramolecular interactions and hence cocrystal formation[15]. Two different polymorphic forms of the cocrystal composed of one molecule of SDM and one molecule of 4-ASA have been reported[10,16]. The hypothesis underpinning this work is that cocrystal engineering can be used to improve the physicochemical properties of the SDM

and also the dosage form manufacturing process, by changing the crystal habit. The combination of the effects of both polymorphic forms and crystal habits on biopharmaceutical properties, such as dissolution, and derived powder properties such as flowability and compaction, still remains poorly understood. For this reason, the aim of this work was to engineer SDM:4-ASA cocrystals with different polymorphic forms and crystal habits in order to investigate the effect on dissolution, wettability, flow and compaction properties. Comparative solid-state characterization was also performed using thermal analysis, powder X-ray diffraction, helium pycnometry, laser diffraction, specific surface area analysis and scanning electron microscopy.

2. Materials and methods

2.1. Materials

SDM and 4-ASA, with a purity ≥ 99%, were purchased from Sigma–Aldrich (Wicklow, Ireland). Ethanol and acetone were supplied from Corcoran Chemicals (Dublin, Ireland). HPLC grade methanol was purchased from Fisher Scientific (Dublin, Ireland). Potassium hydrogen phosphate was obtained from Sigma–Aldrich (Wicklow, Ireland) and phosphoric acid from Merck (Darmstadt, Germany). Polyvinylpyrrolidone (PVP K90) was a gift from BASF (Ludwigshafen, Germany).

2.2. Methods

2.2.1. Preparation of polymorphic forms and habits of SDM:4-ASA cocrystal

All cocrystals were prepared using a 1:1 molar ratio (SDM:4-ASA).

Cocrystal Polymorph I: liquid-assisted milling

Liquid-assisted co-milling was carried out in a Retsch PM100 planetary ball mill (Haan, Germany) using three stainless steel balls (Ø=20 mm) in each milling jar (50 ml). Five drops of ethanol were added to the solid mix (1289.2 mg of SDM and 710.67 mg of 4-ASA) using a 3.5 ml disposable transfer pipette (Fisher Scientific, Dublin, Ireland) prior to milling. The rotation speed of the solar disk was set to 400 rpm. Total milling time was 35 min. A pause period of 5 min was made after 15 min of milling in order to avoid high temperature in the jar and thus the risk of melting/decomposition of the compounds[10].

Cocrystal Polymorph II- Habit I: Crystallization from ethanol

Polymorph II-Habit I was prepared as previously described by Grossjohann et al.[10] with a few modifications. 4-ASA (153.4 mg) was dissolved in ethanol (40 ml) in a round bottom flask. Afterwards, SDM (278.3 mg) was added to the solution and another 10 ml of ethanol were incorporated. Water bath sonication (10 s) followed by microwaving (10 s) were required to ensure complete dissolution. Ethanol was evaporated using a rotavapor (Buchi, Flawil, Switzerland) at 250 mbar pressure and 55 °C. Immediately after solvent

evaporation, the flask was removed in order to avoid a colour change from white to brownish. The flask was kept in the oven at 50 °C for 5 min to remove any residual solvent left and then the powder was recovered.

Cocrystal Polymorph II- Habit II: Crystallization from acetone

4-ASA (153.4 mg) was dissolved in acetone (40 ml) in a round bottom flask. Afterwards, SDM (278.3 mg) was added to the solution and another 10 ml of acetone was incorporated. The rest of the process was identical to that described above.

Cocrystal Polymorph II- Habit III: Crystallization from ethanol followed by dry milling

Powder obtained after solvent evaporation using ethanol was milled in a Retsch PM100 planetary ball mill (Haan, Germany) using three stainless steel balls (Ø=20 mm) in a 50 ml milling jar. A sample mass of 2 g of Polymorph II-Habit I was used. The rotation speed of the solar disk was set to 400 rpm and the total milling time was 10 min.

Cocrystal Polymorph II- Habit IV: Spray-drying

Spray drying was performed using a Buchi B-290 Mini Spray Dryer (Buchi, Flawil, Switzerland) operating in the open-mode. Solution concentrations of 1% (w/v) of SDM:4-ASA (1:1 molar ratio, 644.6 and 355.3 mg respectively) were prepared using ethanol (100 ml). The solutions were delivered to a 2-fluid nozzle (0.7 mm nozzle tip and a 1.5 mm diameter nozzle screw cap) using a peristaltic pump at a speed of 30% (9–10 ml/min). Nitrogen (at 6 bar) was used as the drying gas in a co-current mode with aspirator capacity set to maximum (100%). The flowmeter for the standard 2-fluid nozzle was set at 4 cm which is equivalent to 473 NL/h. The inlet temperature was fixed at 78°C and the outlet temperature varied between 50°C and 57°C[10].

Physical mixture

4ASA (153.4 mg) and SDM (278.3 mg) raw materials were manually mixed using a mortar and pestle in a molar ratio 1:1.

2.2.2. Physicochemical characterisation

Powder X-ray diffraction (PRXD)

Powder X-ray analysis was performed using a Miniflex II Rigaku diffractometer with Ni-filtered Cu Kα radiation (1.54 Å). The tube voltage and tube current used were 30 kV and 25 mA, respectively. The PXRD patterns were recorded (n=3) from 5° to 40° on the 2 theta at a step scan rate of 0.05° per second[17]. Rigaku Peak Integral software was used in the determination of peak intensity for each sample using the Sonnefelt-Visser background edit procedure.

Differential scanning calorimetry (DSC)

Differential scanning calorimetry was performed using a Mettler Toledo DSC 821e instrument under nitrogen purge. Sample powders (4-6 mg) were placed in aluminium pans (40 µl), sealed, pierced to provide three vent holes and heated at a rate of 10 °C/min in the temperature range of 25 to 220 °C. Calibration of the instrument was carried out using indium as standard. The DSC system was controlled by Mettler Toledo STARe software (version 6.10) working on a Windows NT operating system. Temperatures of melting events (n=3) refer to onset temperatures[10].

Particle size distribution analysis (PSD)

The geometric particle size distributions (PSD) were determined by laser diffraction using a Malvern Mastersizer 2000 (Malvern Instruments Ltd., Worcestershire, U.K.). Particles were dispersed using a Scirocco dry feeder instrument with 1 bar pressure. An obscuration of 1−6% was obtained under a vibration feed rate of 50%. Liquid measurements in deionised water were also carried out using a Hydro 2000 µP accessory (for small volume wet sample dispersions) at 2000 rpm. Data were analysed based on the D10, D50, D90 and the span of the PSD. Results reported are the average of three analyses.

Surface area measurements

To determine the specific surface area (TBET) by the Brunauer, Emmett, Teller (BET) isotherm method, a Micromeritics Gemini VI 2385C (Micromeritics, Norcross, GA, USA) surface area analyser was used. The amount of nitrogen adsorbed at 6 relative pressure points in the relative pressure (P/P_o) range of 0.05 to 0.3, with an equilibration time of 10 s, was used for the BET analysis. Each average result is calculated on the basis of three measurements. Free space was determined separately for each sample using helium gas. Saturation pressure P_o was determined prior to the measurement of each sample[18]. Samples were prepared by purging under N_2 overnight at 25 °C.

Density measurements

The true density was measured by an Accupyc 1330 Pycnometer (Micromeritics, Norcross, GA, USA) using helium (99.995% purity) to determine the volume of the sample. Samples were dried under N_2 atmosphere prior to measurement for 24 h at 25 °C[18]. A 5 cm^3 graduated cylinder was used in the bulk density (aerated density) determination of samples. The container was filled with accurately weighed sample and the top was levelled. The density was calculated as the ratio of the mass to the volume of the sample. The tap density was determined similarly to the aerated density, but the volume taken for calculations was that after 300 strokes. Each average result is calculated on the basis of three measurements. Carr's compressibility index was calculated using the bulk and tap density values according to the following equation[19]:

Carr's compressibility index = (tap density − bulked density)/ tap density ×100 (Eq. 1)

Scanning electron microscopy (SEM)

Surface images of powders were performed at various magnifications by SEM using a Zeiss Supra Variable Pressure Field Emission Scanning Electron Microscope (Germany)

equipped with a secondary electron detector at 5 kV. Samples were glued onto aluminium stubs and sputter-coated with gold under vacuum prior to analysis.

Wettability studies

Compacts were prepared by compressing powder (300 mg) using a Perkin Elmer hydraulic press. A 13 mm punch and die set at a pressure of 8 tonnes for 1.5 min was used. Compacts were placed on a stage and raised to an appropriate level. Contact angles made by deionised water with the compacts were measured using the sessile drop method on a drop shape analyser (FTA 125, First Ten Angstrom, Virginia, USA) From a captured video, the contact angle was calculated based on the Young-Laplace equation[20]. The slope of the tangent to the drop at the liquid−solid−vapor interface line was calculated. All measurements were performed in triplicate under ambient conditions of 25 ± 2 °C[7].

2.2.3. Compaction studies at a single compression force

Biconvex tablets (n=10, 200 mg) were compressed using a Natoli NP-RD10 (Saint Charles, USA) laboratory scale single punch tablet press supplied with an Enerpac (USA) AC RC53 piston working in the range from 0 to 10 tons and standard concave 10 mm diameter punch and die tooling. Pressure was released immediately after the desired compression pressure was reached. Tablets were pushed out of the die using the bottom punch. To lubricate the tablet press tooling, the die and upper punch were dusted, using a paint brush, with magnesium stearate. A set of ten tablets was subjected to radial hardness testing using a Dr. Schleuniger, Pharmatron, model 6D tablet tester. Compaction properties were quantified in terms of hardness achieved at the applied compaction pressure of 6 KN. Also, it was monitored whether or not the tablet capped under the applied pressure and if the breakage of the tablet occurred in a consistent manner[18].

2.2.4. Flow-through cell dissolution studies

A single flow-through cell dissolution apparatus (Sotax) in an open-loop configuration with an internal diameter of 12 mm was used. One ruby bead of about 5 mm was positioned at the apex of the bottom cone to equalize the jet of fluid entering the cell. Powder was loaded into the flow-through cell as illustrated in Figure 1.

The powder to be examined was sieved through a 300 µm sieve before performing the dissolution study. The amount of powder loaded in every study was 300 mg. A cellulose Whatman® filter grade 1 (11 µm), a glass microfiber filter (Whatman® GF/D, 2.7 µm), a glass microfiber Whatman® filter grade GF/F (0.7 µm) and a hydrophilic membrane Pall Supor® (0.45 µm) were positioned sequentially at the inner top of the cell to retain undissolved material. The dissolution medium was pumped (120 pulses per minute) through the cell at a flow rate of 8 ml/min over 180 min. Studies were performed using two different media: i) deionised water (pH 5.5) and ii) deionised water (pH 5.5) with 0.1% PVP K90. The temperature was maintained at 37 ± 0.5 °C during testing. Samples were collected from the flow-through cell at different time points (every 5 min from 0 to 30 min, every 10 min from 30 to 60 min and every 15 min from 60 to 180 min) and then

were diluted with mobile phase and analysed by HLPC (method described below) to calculate the percentage of drug dissolved at each time point.

Flow-through cell PXRD studies

Samples were collected from the inside of the cell at different time points, dried at ambient temperature under a nitrogen atmosphere and analysed by PRXD.

2.2.5. Quantification by HPLC

The concentration of SDM and 4-ASA was determined using an Alliance HPLC with a Waters 2695 Separations module system and Waters 2996 Photodiode array detector. The mobile phase consisted of methanol/buffer pH 6.5 40/60 (v/v). The buffer was prepared from a 50 mM dipotassium phosphate solution adjusted to pH 6.5 with phosphoric acid. The mobile phase was vacuum filtered through a 0.45 µm membrane filter (Pall Supor® 0.45 µm, 47 mm) and bath sonicated for 5 min. Separation was performed on a Phenomenex Inertsil ODS (3) C18 column (150 mm length, diameter 4.6 mm, particle size 5 µm) at a UV detection wavelength of 265 nm with an injection volume of 20 µL. The elution was carried out isocratically at ambient temperature with a flow rate of 1 ml/min. The total run time per sample was 6 min. Elution times for 4ASA and SD were 1.9 min and 4.0 min respectively. For peak evaluation Empower software was used. The calibration curves were linear for both components between 100 µg/ml – 0.05 µg/ml (R^2 > 0.9999). The linear regression calibration curve obtained for 4ASA was y= 91157x +8454.8 and for SD was y= 80548x + 3498.7.

2.2.6. Mechanistic mathematical models

In order to investigate the release from the different cocrystal habits, the dissolution data obtained was fitted using the following kinetic equations[21,22]: first order (Eq. 2), Hixson–Crowell (Eq. 3) and Korsmeyer–Peppas (Eq. 4):

$$\ln Q_t = \ln Q_0 + K_1 t \qquad \text{(Eq.2)}$$

$$Q_\infty^{1/3} - (Q_\infty - Q_t)^{1/3} = K_s t \qquad \text{(Eq. 3)}$$

$$\frac{Q_t}{Q_\infty} = K_{KP} t^n \qquad \text{(Eq. 4)}$$

Where Q_t is the amount of drug dissolved in time t, Q_0 is the initial amount of drug in the solution (most times, Q_0=0), Q_∞ is the initial amount of drug in the tablet; $\frac{Q_t}{Q_\infty}$ is the fraction of drug release at time t; K_1 is the first order release constant, Ks is a constant incorporating the surface-volume relation; K_{KP} is a constant that describes the structural and geometric characteristics of the drug dosage form; n is the release exponent which describes the drug release mechanism. The n can have a value of 0.5, 0.45 or 0.43 when the particle shape is a thin film, a cylinder or a sphere respectively which corresponds to

Fickian release controlled by diffusion. Anomalous non-Fickian transport is described when n is between those values and 1 ($0.5 < n < 1$ for thin films, $0.45 < n < 1$ for cylinder and $0.43 < n < 1$ for spheres). n=1 corresponds with zero order release[23]. To test the applicability of the drug release model, the regression coefficient (R^2) was used[21,24].

2.2.7. Molecular modelling

The program Mercury (version 3.5.1., Cambridge Crystallographic Data Centre, Cambridge, UK) was used for calculation of X-ray powder patterns on the basis of the single crystal structure. Miller's indices of various facets of the crystal were identified using Mercury and it was also used to visualise the molecular arrangement on different crystal facets of the cocrystal.

2.2.8. Statistical analysis

Statistical analysis was performed via one-way ANOVA Test using Minitab 16 (Minitab Ltd, Coventry, UK) followed by Tukey's test considering p-values for statistical significance < 0.05. Linear regression analysis was performed using the method of least squares by Microsoft® Excel software. The adequacy of the fit was assessed from the regression coefficient (R^2).

3. Results and discussion

3.1. Preparation and characterisation of SDM:4-ASA polymorphic cocrystals and crystal habits

Polymorph I was successfully produced by liquid-assisted milling while polymorph II was obtained after crystallisation from different solvents (ethanol or acetone) or spray-drying. The yield was higher than 75% in all the manufacturing processes apart from spray drying, which resulted in 45% yield.

Results of thermal analysis are shown in Figure 2A and Table 1. DSC results showed that the melting point of the polymorphm I and II was between those of SDM (T_m = 197.1 ± 0.1) and 4-ASA (T_m = 145.6 ± 0.4). The 1:1 molar ratio was employed in the preparation of the different polymorphic forms and crystal habits because a single melting event was obtained unlike the non-equimolar mixtures as previously described by Grossjohann et al.[10]. The equimolar physical mixture also exhibited a single melting point that was between the single components but it was shifted to lower temperatures (T_m = 159.8 ± 0.7). The melting point of the five cocrystals was between 166 and 171 °C.

PXRD analysis showed that all the diffraction peaks of the equimolar physical mixture of SDM and 4-ASA could be superimposed with those of the two individual components (Figure 2B). However, the diffractograms of both polymorphic cocrystals of SDM and 4-

ASA showed patterns with characteristic diffraction peaks which differ between one another and also differ from those of the single components. Bragg peak positions of polymorph II was the same in all the crystal habits (I to IV). However, the peak intensity varied, indicating different preferred orientation of the crystallographic planes (Fig 2B). The peak area, relating to the degree of crystallinity of the polymorph I and polymorph II (habit I to IV) was 6189, 4541, 4977, 4306 and 3871 expressed as intensity (arb. units)/2 θ degrees respectively which showed a reduction in the degree of crystallinity after spray drying (habit IV) and solvent evaporation followed by milling (habit III). A graphical presentation of XRPD peak intensities of prominent planes in Polymorph II- Habits I – IV is shown in Figure 3. The intensity of (1,2,1) and (3,0,1) facets was increased after spray drying whereas after milling, the facet (1,1,0) was also prominent. Polymorph II-Habit II showed characteristic prominent (5,0,1) and (1,2,1) facets whereas habit I exhibited (2,0,2) and (3,0,1) facets of higher intensity. Polymorph I exhibited prominent (0, 1, -1) and (2, 0, -2) facets.

SEM micrographs clearly showed the difference in the crystal habits: small prismatic crystals (Polymorph I), large prismatic crystals (Polymorph II-habit I), large plate-like crystals (Polymorph II-habit II), small cube like-crystals (Polymorph II-habit III) and microspheres (Polymorph II-habit IV) (Figure 4). The crystal habit of the physical mixture was a mixture of the crystal habits of the single components.

Particle size distribution analysis showed that the spray dried sample (polymorph II-Habit IV) had the smallest median particle size (D_{50}) 5.7 ± 0.7 µm which corresponds with the highest surface area (3.669 ± 0.011 m^2/g) (Table 1), whereas the polymorph II- habit II exhibited the largest D_{50} (60.5 ± 6.2 µm) and the lowest surface area (0.758 ± 0.065 m^2/g). The median particle size of the polymorph II- habit I was 2-3 fold lower than polymorph II-habit III and polymorph I. However, both polymorph II-habit III and polymorph I exhibited higher surface areas than polymorph II-habit I (1.694 and 2.830 m^2/g versus 1.136 m^2/g), which could be due to the fact that the bigger aggregates consisted of crystals of smaller size, as can be observed in the SEM micrographs (Fig. 4).

3.2. Carr's Compressibility Index and compaction properties

Tabletability can be defined as the capacity of a powdered material to be transformed into a tablet of specified strength under the effect of compaction pressure[25]. Ideally, the target for pharma companies would be to engineer a crystal habit that is suitable for direct compression with only a low amount of excipients, which forms a stable compact at low punch forces, has good flowability and a low tendency to stick to punches.

Differences in Carr's compressibility Index (as an indicator of flow) and compaction properties between the polymorphs and habits are shown in Table 1. The differences in bulk density may be related to differences in crystal habits which lead to different contact points and frictional and cohesive forces between crystals. In general, the lower Carr´s compressibility index, the better the flow[26]. All the cocrystals examined demonstrated relatively poor flow, with Carr's Compressibility Indices greater than 30% in all cases.

For this reason, further powder rheometry studies were not performed. Polymorph II-habit I exhibited the highest Carr's index (43.9 ± 3.1%) indicative of poorest flowability, similar to the physical mixture of the single components, which could be due to its crystal habit, which is characterised by large prismatic crystals with pointed edges. Polymorph II- habit IV also showed very poor flow (38.9 ± 4.5%), probably due to the small particle size and also the manufacturing process (spray drying) that frequently leads to electrostatic charged powders.

A decrease in particle size enhanced the compact hardness, due to smaller crystals having a larger number of contact points between crystals in the compacts[27]. Similar observations have been previously reported in sulfamerazine polymorphs by other authors[28]. Spray dried (polymorph II- habit IV) and milled materials (polymorph I and polymorph II – habit III) resulted in compacts with increased hardness and less tendency to cap. Cocrystals obtained by solvent evaporation (polymorph II- habits I & II) exhibited significantly poorer compaction properties indicating weak bonding between particles and difficulty to orient in different directions and fracture during tableting, which could be related to their crystal shape (large prismatic and plate-like crystals).

3.3. Dissolution studies and wettability

The equimolar physical mixture exhibited the fastest dissolution rate at earlier time points (0-10 min) when the release of both 4-ASA and SDM was taken into account (Fig. 5a). However, it can be observed in Fig. 5b that the dissolution was incongruent, resulting in much larger and faster release of 4-ASA compared to SDM. The fast dissolution of the physical mixture is in good agreement with the wettability results in Table 1 and as shown by other authors, the wettability of a powder can be reliably estimated by the contact angle measured on compressed powder[29]. The lower contact angle of the physical mixture can be related to its higher surface hydrophilicity. 4-ASA is a more hydrophilic compound (water solubility= 2 g/L at 20 °C[30]) than SDM (water solubility= 1.5 g/L at 29 °C[31]) but also than the cocrystals, leading to a good wettability that affects the dissolution at initial times. However, wettability is not a good tool to assess the overall dissolution profile at longer periods of time. The amount of SDM dissolved from the physical mixture at 60 min in water at 37 °C was 2.5-fold lower compared to polymorph I and polymorph II-habit III.

The overall amount dissolved at 60 min was higher for polymorph I & polymorph II-habit III followed by polymorph II-habit I> polymorph II-habit II> physical mixture > polymorph II-habit IV (Fig 5a). Surprisingly, polymorph II-habit IV displayed the lowest dissolution rate in spite of having the smallest particle size and highest surface area. To investigate this fact, the particle size analyses of the samples suspended in deionised water as medium were performed, showing a dramatic particle aggregation for the polymorph II-habit IV (D_{50}= 1042.3 ± 11.6 µm) and also but to a lesser extent for the polymorph II-habit II (D_{50}= 172.5 ± 5.0 µm). Another factor that explains the different dissolution profile among cocrystals is the polymorphic transitions that can occur in situ during dissolution. Polymorph II- habit III was transformed rapidly (after 1 min) into polymorph

I during dissolution, as was confirmed by PXRD due to the presence of a prominent peak at 10.25 2θ degrees (Fig. 6a). Its small particle size (and therefore high solid-solvent interfacial contact area) and its manufacturing process, which was similar to that of the polymorph I, could explain why the polymorphic transition occurred, resulting in an almost identical dissolution profile. Polymorph II-habit IV was partially transformed into polymorph I, which could also be related to the small particle size and higher surface area that facilitates the polymorphic transformation. However, an extra peak at 9.35 2θ degrees corresponding to SMD was also observed, which could explain why the dissolution rate was slowed down. Polymorph II-habit I was stable during the entire dissolution test whereas polymorph II-habit II showed the presence of both peaks at 10.25 and 9.35 2θ degrees at early time points (1 min) which were not detected at longer times, but this may explain why the dissolution rate for polymorph II- habit II was slower than polymorph II-habit I (Fig. 5a).

Both polymorph I and polymorph II-habit III cocrystals exhibited congruent dissolution, characterised by an equimolar release for SDM and 4-ASA over time (Fig. 5b). However, the dissolution was incongruent, not only for the physical mixture, but also for the other three cocrystals due to the faster release of 4-ASA (for polymorph II- habit I & II) or the faster release of SDM (for polymorph II-habit IV).

Using low polymer concentrations like PVP has been used as a successful strategy to minimise particle aggregation and inhibit precipitation from a supersaturated solution[32-34]. For this reason, further dissolution experiments were performed by adding 0.1% w/w PVP to the dissolution medium (Fig. 5c). The dissolution rate of polymorph II-habit IV was significantly enhanced at early time points (0-20 min) resulting in a 3.3-fold higher amount of SDM dissolved at 60 min. This can be explained by the fact that particle agglomeration was inhibited by the presence of PVP. The dissolution rate of polymorph II-habit I was also slightly increased in PVP although the same percentage of cocrystal was dissolved in both media at 60 min. Nevertheless, in the case of polymorph II-habit II there was a dramatic 13-fold reduction in the amount of SDM dissolved after 60 min when PVP was used. This could be due to the preparation process, which involves acetone as solvent. Further investigation is required to identify if traces of acetone in the cocrystal could lead to PVP precipitation in the surroundings of the particles at earlier time points, or if some other phenomenon explains the hindered release.

The addition of PVP prevented incongruent dissolution and maintained the release of both cocrystal components resulting in an equimolar dissolution (Fig. 5d). Free SDM was not detected during the dissolution process in any of the cocrystals, as confirmed by PXRD (Fig 6b). Nevertheless, polymorph II-habit III was also transformed into polymorph I in the presence of PVP. It appears that, not only does the smaller particle size, that presents a larger surface area to the dissolution medium, trigger the polymorphic transition, but also the manufacturing process is crucial in determining the stability of the polymorph II. Hence, depending on process conditions a manufacturing process could produce different habits which could lead to different polymorphic transitions.

3.4. Mathematical modelling

The results of the curve fitting to the different mathematical models for dissolution in both deionised water and water/PVP 0.1 % (w/v) are shown in Table 2. From comparison of the regression coefficients, it was found that the Hixson-Crowell model provided a good fit for all the cocrystals, except for physical mixture where the Korsmeyer-Peppas model provided a better fit.

The Hixson-Crowell model, also called the cube root law, applies to pharmaceutical dosage forms, where the dissolution takes place in planes that are parallel to the drug surface if the particle dimensions diminishes proportional in a way that the initial geometrical form keep constant all the time[21]. The application of the release profiles to Hixson-Crowell model indicates that a change in surface area and diameter of the particles occur with progressive dissolution as a function of time[35]. The major disadvantages of this model are: i) sink conditions are required, ii) the geometry of the dissolving particles is considered spherical and without any change over time and iii) the particles remain intact and do not disintegrate into smaller fragments during dissolution[22]. The first assumption is usually correct during the flow-through cell dissolution studies as an open-loop system was used, however, the other two assumptions may not be valid, which can lead to deviations from the models. This was the case for the physical mixture, probably because the geometrical shape of the particles is far from spherical. In this case, the Korsmeyer-Peppas model provided a better fit where the release exponent (n) was 0.29. A value of $n \leq 0.43$ indicates a time dependence of drug release by Fickian diffusion from a thin film. The physical mixture is a two component system where one of the components (4-ASA) is more soluble than the other one (SDM). During the dissolution experiment, the formation of a very large aggregate, similar to a matrix system, was observed over time. Therefore, SDM release was hindered as SDM molecules have to diffuse from this system in order to be dissolved, which could explain this type of release.

3.5. Molecular modelling

The visualisation of the cocrystal packing along the axis a and c is represented in Figure 7. The main functional groups that can contribute to the surface chemistry are $–NH_2$, -OH and –COOH in the 4-ASA and the $–SO_2$ and $-NH_2$ in the SDM. Face indexation data revealed that the relative abundance of major facets on the surface chemistry differed significantly among the four crystal habits of polymorph II (Fig. 3). The percent contribution of (1,1,0) facet on the surface of the polymorph II-habit III was higher compared to the other habits. The presence of hydrophilic groups (such as $-SO_2$) at this facet could explain the faster dissolution kinetics (Fig 7b). Similarly, the (0,1,-1) facet corresponding to the prominent peak at 10.25 2θ degrees in the polymorph I is characterised by the presence of $–SO_2$ (Fig. 7c). In addition, both polymorph I and polymorph II-habit III had the same contact angle, which is indicative of similar functional groups at the surface chemistry leading to similar dissolution profiles both in water and water/PVP.

4. Conclusions

A specific crystal habit can be the result of multiple factors during the manufacturing process. However, the crystal habit can have a great influence on the physicochemical properties of the drug. Even for cocrystals with poor pharmaceutical characteristics, a habit can be engineered that results in better flowability, tableting and dissolution behaviour. Milling and spray drying resulted in powders with enhanced hardness due to the smaller particle size but only milled materials led also to acceptable flow, as spray dried powders were electrostatically charged hindering the flowability. The dissolution properties were also affected by the cocrystal habit resulting in a higher overall dissolution rate in deionised water for milled powders followed by powders obtained by crystallization from solution and then by spray drying. In spite of the spray dried powder exhibiting better micromeritic characteristics for dissolution (smaller particle size and higher surface area), it suffered from agglomeration, which notably reduced its dissolution rate in water, relative to other crystal habits examined. However, the presence of 0.1% w/v of PVP in the medium had a large impact on inhibiting particle agglomeration and then enhancing the dissolution of the spray dried cocrystal.

5. Acknowledgements

This publication has emanated from research conducted with the financial support of Science Foundation Ireland under Grant Number SFI/12/RC/2275.

Figure captions

Figure 1. Schematic diagrams showing the position of the powder in the flow-through cell.

Figure 2. DSC thermograms and PXRD patterns of SDM: 4-ASA (1:1 molar ratio) cocrystal and unprocessed materials. A) DSC thermograms; B) PXRD patterns. Key: a) Unprocessed SDM; b) Unprocessed 4-ASA; c) Physical mixture; d) Polymorph I; e) Polymorph II-Habit I; f) Polymorph II-Habit II; g) Polymorph II- Habit III and h) Polymorph II-Habit IV.

Figure 3. Graphical presentation of PXRD peak intensities of prominent planes in Polymorph II- Habits I -IV. Key: -♦- Polymorph II-Habit I; **-■**-Polymorph II-Habit II; **-▲**- Polymorph II- Habit III and -x- Polymorph II-Habit IV.

Figure 4. SEM micrographs of unprocessed API (sulfadimidine) and coformer (4-ASA) and cocrystals.

Figure 5. Dissolution profiles and stoichiometry of dissolution of different polymorphs and crystal habits at 37°C.

A) Dissolution profiles in deionised water. Key: Physical mixture **(- -●- -);** Polymorph I (- -♦- -); Polymorph II- Habit I (—■—); Polymorph II- Habit II(—▲—); Polymorph II- Habit III(—♦—) and Polymorph II- Habit IV (—●—) .

B) Stoichiometry during dissolution in deionised water. Key: Closed symbols refer to SDM release and open symbols refer to 4-ASA release. Physical mixture [SDM **(- -●- -**), 4-ASA**(- -○- -)];** Polymorph I [SDM (- -♦- -), 4-ASA (- -◊- -)]; Polymorph II- Habit I [SDM (—■—),4-ASA (—□—)]; Polymorph II- Habit II [SDM (—▲—), 4-ASA (—Δ—)]; Polymorph II- Habit III [SDM (—♦—), 4-ASA (—◊—)], and Polymorph II- Habit IV [SDM (—●—), 4-ASA (—○—)].

C) Comparison of dissolution profile in deionised water and water/PVP 0.1%. Key: Polymorph I, in water (- -♦- -), in water/PVP (- -◊- -); Polymorph II- Habit I, in water (—■—),in water/PVP (—□—); Polymorph II- Habit II, in water (—▲—), in water/PVP (—Δ—); Polymorph II- Habit III in water (—♦—), in water/PVP (—◊—), and Polymorph II- Habit IV, in water (—●—), in water/PVP (—○—).

D) Stoichiometry during dissolution in deionised water/ PVP 0.1%. Key: Closed symbols refer to SDM release and open symbols refer to 4-ASA release. Polymorph I [SDM (- -♦- -), 4-ASA (- -◊- -)]; Polymorph II- Habit I [SDM (—■—),4-ASA (—□—)]; Polymorph II- Habit II [SDM (—▲—), 4-ASA (—Δ—)]; Polymorph II- Habit III [SDM (—♦—), 4-ASA (—◊—)], and Polymorph II- Habit IV [SDM (—●—), 4-ASA (—○—)].

Figure 6. Comparison of PXRD patterns before and after dissolution. A) In water at 37°C. B) In water/PVP 0.1% at 37°C.

Figure 7. Visualization of crystal structure and molecular surface packing. Key: A) Crystal structure of SDM:4-ASA 1:1 polymorph II cocrystal viewed along the *c* axis; B) visualization of molecular surface packing of polymorph II along with surface chemistry of (110) facet using Mercury 3.5.1. software and C) visualization of molecular surface packing of polymorph I along with surface chemistry of (0,1,-1) facet using Mercury 3.5.1. software.

References

1. Babu NJ, Nangia A. Solubility advantage of amorphous drugs and pharmaceutical cocrystals. *Cryst Growth Des* 2011; 11: 2662-2679.
2. Serrano Lopez DR, Lalatsa A. Peptide pills for brain diseases? Reality and future perspectives. *Therapeutic delivery* 2013; 4: 479-501.
3. Blagden N*, et al.* Crystal engineering of active pharmaceutical ingredients to improve solubility and dissolution rates. *Advanced drug delivery reviews* 2007; 59: 617-630.
4. Miroshnyk I*, et al.* Pharmaceutical co-crystals-an opportunity for drug product enhancement. *Expert opinion on drug delivery* 2009; 6: 333-341.
5. Chadha R*, et al.* Pharmaceutical cocrystals: a novel approach for oral bioavailability enhancement of drugs. *Critical reviews in therapeutic drug carrier systems* 2012; 29: 183-218.
6. Qiao N*, et al.* Pharmaceutical cocrystals: an overview. *International journal of pharmaceutics* 2011; 419: 1-11.
7. Modi SR*, et al.* Impact of Crystal Habit on Biopharmaceutical Performance of Celecoxib. *Cryst Growth Des* 2013; 13: 2824-2832.
8. Bansal SS*, et al.* Molecular and thermodynamic aspects of solubility advantage from solid dispersions. *Molecular pharmaceutics* 2007; 4: 794-802.
9. Alhalaweh A*, et al.* Theophylline cocrystals prepared by spray drying: physicochemical properties and aerosolization performance. *AAPS PharmSciTech* 2013; 14: 265-276.
10. Grossjohann C*, et al.* Polymorphism in Sulfadimidine/4-Aminosalicylic Acid Cocrystals: Solid-State Characterization and Physicochemical Properties. *Journal of pharmaceutical sciences* 2015.
11. Stoica C*, et al.* Understanding the Effect of a Solvent on the Crystal Habit. *Crystal Growth & Design* 2004; 4: 765-768.
12. Modi SR*, et al.* Effect of Crystal Habit on Intrinsic Dissolution Behavior of Celecoxib Due to Differential Wettability. *Cryst Growth Des* 2014; 14: 5283-5292.
13. Rasenack N, Muller BW. Crystal habit and tableting behavior. *International journal of pharmaceutics* 2002; 244: 45-57.
14. Huovinen P*, et al.* Trimethoprim and sulfonamide resistance. *Antimicrobial agents and chemotherapy* 1995; 39: 279-289.
15. Caira MR. Sulfa drugs as model cocrystal formers. *Molecular pharmaceutics* 2007; 4: 310-316.
16. Caira MR. Molecular complexes of sulphonamides 2. 1:1 complexes between drug molecules: Sulfadimidine-acetylsalicylic acid and sulfadimidine-4-aminosalicylic acid. *J Crystallogr Spectrosc Res* 1992; 22: 193-200.
17. Mugheirbi NA*, et al.* Heat induced evaporative antisolvent nanoprecipitation (HIEAN) of itraconazole. *International journal of pharmaceutics* 2014; 471: 400-411.
18. Paluch KJ*, et al.* Impact of alternative solid state forms and specific surface area of high-dose, hydrophilic active pharmaceutical ingredients on tabletability. *Molecular pharmaceutics* 2013; 10: 3628-3639.
19. Tajber L*, et al.* Spray drying of budesonide, formoterol fumarate and their composites-II. Statistical factorial design and in vitro deposition properties. *International journal of pharmaceutics* 2009; 367: 86-96.
20. Stalder AF*, et al.* Low-Bond Axisymmetric Drop Shape Analysis for Surface Tension and Contact Angle Measurements of Sessile Drops. *Colloids and Surfaces A: Physicochemical and Engineering Aspects* 2010; 364: 72-81.
21. Costa P, Sousa Lobo JM. Modeling and comparison of dissolution profiles. *European journal of pharmaceutical sciences : official journal of the European Federation for Pharmaceutical Sciences* 2001; 13: 123-133.
22. Siepmann J, Siepmann F. Mathematical modeling of drug dissolution. *International journal of pharmaceutics* 2013; 453: 12-24.

23. Lao LL*, et al.* Modeling of drug release from bulk-degrading polymers. *International journal of pharmaceutics* 2011; 418: 28-41.
24. Mamani PL*, et al.* Matrix tablets: the effect of hydroxypropyl methylcellulose/anhydrous dibasic calcium phosphate ratio on the release rate of a water-soluble drug through the gastrointestinal tract I. In vitro tests. *AAPS PharmSciTech* 2012; 13: 1073-1083.
25. Khomane KS, Bansal AK. Effect of particle size on in-die and out-of-die compaction behavior of ranitidine hydrochloride polymorphs. *AAPS PharmSciTech* 2013; 14: 1169-1177.
26. Carr JR. Classifying flow properties of solids. *Chem Eng* 1965; 72: 69-72.
27. Sun C, Grant DJ. Effects of initial particle size on the tableting properties of L-lysine monohydrochloride dihydrate powder. *International journal of pharmaceutics* 2001; 215: 221-228.
28. Sun C, Grant DJ. Influence of crystal structure on the tableting properties of sulfamerazine polymorphs. *Pharmaceutical research* 2001; 18: 274-280.
29. Dahlberg C*, et al.* Surface composition and contact angle relationships for differently prepared solid dispersions. *European journal of pharmaceutics and biopharmaceutics : official journal of Arbeitsgemeinschaft fur Pharmazeutische Verfahrenstechnik eV* 2008; 70: 478-485.
30. 4-amino salicylic physicochemical porperties. Chemical book. Available at: http://www.chemicalbook.com/ChemicalProductProperty_EN_CB9679687.htm. Date of access: 08/03/2015.
31. Sulfadimidine drug bank database. Available at: http://www.drugbank.ca/drugs/DB01582. Date of access: 08/03/2015.
32. Warren DB*, et al.* Using polymeric precipitation inhibitors to improve the absorption of poorly water-soluble drugs: A mechanistic basis for utility. *Journal of drug targeting* 2010; 18: 704-731.
33. Guzmán H*, et al.* Combined use of crystalline salt forms and precipitation inhibitors to improve oral absorption of celecoxib from solid oral formulations. *Journal of pharmaceutical sciences* 2007; 96: 2686-2702.
34. Gibson M. 2009. Pharmaceutical Preformulation and Formulation 2nd Edition. A practical guide from candidate drug selection to commercial dosage form. ed., New York, USA: Informa Healthcare.
35. Murtaza G*, et al.* Biowaiver study of oral tabletted ethycellulose microcapsules of a bcs class I drug. *Bull Chem Soc Ethiop* 2009; 23: 175-186.

Table 1. Micrometric properties and physicochemical characteristics of 4ASA:SD (1:1 molar ratio) cocrystals form I, form II, physical mixture and raw materials. Key: Melting onset temperatures (**T_m),** heating fusion (**AH_f),** Span calculated as $(D_{90} - D_{10})/D_{50}$, capping expressed as: +++ when more than 5 out of 10 tablets capped under the applied pressure; ++ when 3 or 4 out of 10 tablets capped under the applied pressure; + when 1 or 2 out of 10 tablets capped under the applied pressure and – when 0 out of 10 tablets capped under the applied pressure.

Sample	**Preparation (Yield in %)**	**T_m (°C)**	**AH_f (J/g)**	**BET surface area (m^2/g)**	**Contact angle (°)**	**Hardness (N) / (Capping)**	**True Density (g/cm^3)**	**Bulk density (g/cm^3)**	**Tapped density (g/cm^3)**	**Carr's index (%)**	**D_{10} (µm)**	**D_{50} (µm)**	**D_{90} (µm)**	**Span**
4-ASA	Raw material	145.6 ± 0.4	338.9 ± 2.1	-	-	-	-	-	-	-	-	-	-	-
SDM	Raw material	197.1 ± 0.1	128.7 ± 0.6	-	-	-	-	-	-	-	-	-	-	-
Physical mixture	Mortar and pestle	159.8 ± 0.7	188.9 ± 0.4	0.875 ± 0.025	31.1 ± 2.7	48.9 ± 2.3 (++)	1.49 ± 1.5 x 10^{-3}	0.313 ± 1.1 x 10^{-2}	0.547 ± 3 x 10^{-3}	42.8 ± 2.3	3.7 ± 0.05	9.4 ± 0.5	32.6 ± 0.2	3.1
Polymorph I	Liquid-assisted milling (87.2 ± 3.7)	171.1 ± 1.9	228.6 ± 1.1	2.830 ± 0.003	61.9 ± 2.6	43.3 ± 5.7 (+)	1.45 ± 7 x 10^{-4}	0.373 ± 1.3 x 10^{-2}	0.578 ± 7 x 10^{-3}	35.4 ± 2.9	5.1 ± 0.01	44.9 ± 0.02	266.1 ± 12.1	5.8
Polymorph II – Habit I	Solvent evaporation using EtOH (90.6 ± 4.5)	167.6 ± 0.8	209.4 ± 2.6	1.136 ± 0.012	46.7 ± 2.4	28.1 ± 2.9 (+++)	1.41 ± 1.4 x 10^{-4}	0.216 ± 9 x 10^{-3}	0.385 ± 6 x 10^{-3}	43.9 ± 3.1	3.4 ± 0.03	15.6 ± 0.02	87.7 ± 0.01	5.4
Polymorph II – Habit II	Solvent evaporation using Acetone (81.4 ± 5.6)	167.9 ± 0.8	188.5 ± 2.1	0.758 ± 0.065	73.2 ± 0.1	20.5 ± 5.3 (+++)	1.37 ± 2.1 x 10^{-3}	0.384 ± 0.021	0.554 ± 0.002	30.7 ± 2.8	4.9 ± 0.7	60.5 ± 6.2	273.8 ± 15.2	4.5
Polymorph II – Habit III	Solvent evaporation using EtOH followed by milling (78.6 ± 3.5)	170.2 ± 0.6	212.5 ± 2.3	1.694 ± 0.084	63.4 ± 2.1	53.6 ± 4.4 (-)	1.41 ± 1.1 x 10^{-3}	0.238 ± 0.019	0.346 ± 0.19	31.2 ± 3.3	2.9 ± 0.3	24.8 ± 2.5	180.4 ± 15.9	7.2
Polymorph II – Habit IV	Spray-drying (45.2 ± 3.3)	168.5 ± 0.7	206.3 ± 3.1	3.669 ± 0.011	65.3 ± 1.75	51.2 ± 2.9 (-)	1.41 ± 1.9 x 10^{-3}	0.296 ± 0.015	0.484 ± 0.021	38.9 ± 4.5	1.6 ± 0.1	5.7 ± 0.7	124.3 ± 19.4	21.5

Table 2. Regression coefficient (R^2) values in the analysis of the dissolution data (from 0 to 30 min) for polymorph I, II and physical mixture in water and water/PVP 0.1% at 37 °C using the following kinetic equations: first order, Hixson–Crowell and Korsmeyer–Peppas. Key: n is the release exponent which describes the drug release mechanism.

Cocrystal	Medium	First Order	Hixson–Crowell	Korsmeyer–Peppas (n)
Polymorph I	Water	0.933	0.999	0.996 (0.69)
	Water/PVP	0.917	0.976	0.999 (0.50)
Polymorph II- Habit I	Water	0.943	0.999	0.991 (0.62)
	Water/PVP	0.911	0.996	0.999 (0.61)
Polymorph II- Habit II	Water	0.929	0.986	0.997 (0.50)
	Water/PVP	0.934	0.989	0.993 (0.88)
Polymorph II- Habit III	Water	0.920	0.999	0.997 (0.74)
	Water/PVP	0.915	0.996	0.999 (0.65)
Polymorph II- Habit IV	Water	0.914	0.989	0.986 (0.53)
	Water/PVP	0.869	0.939	0.999 (0.38)
Physical mixture	Water	0.879	0.866	0.994 (0.29)

Figure 1

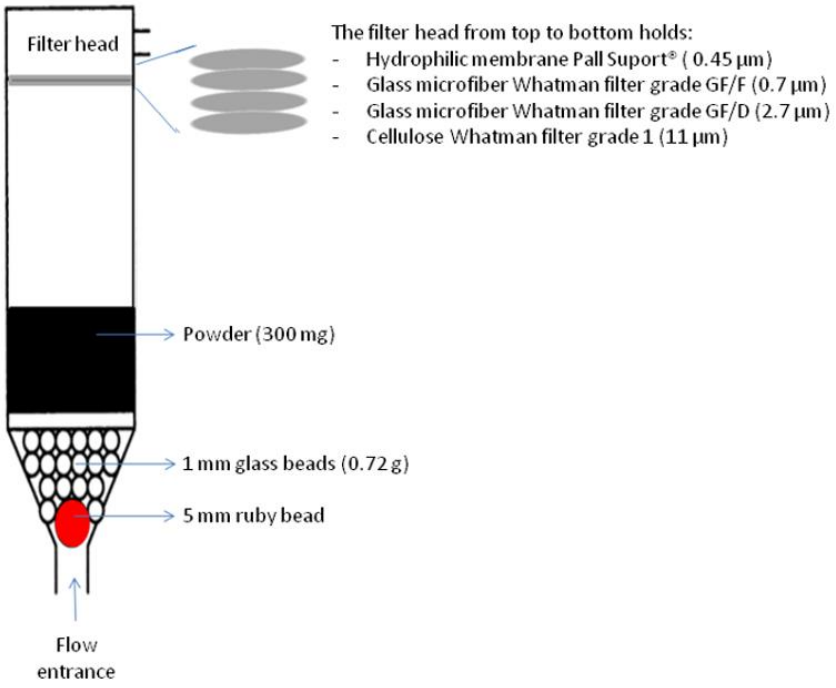
Filter head
The filter head from top to bottom holds:
- Hydrophilic membrane Pall Suport® (0.45 µm)
- Glass microfiber Whatman filter grade GF/F (0.7 µm)
- Glass microfiber Whatman filter grade GF/D (2.7 µm)
- Cellulose Whatman filter grade 1 (11 µm)
Powder (300 mg)
1 mm glass beads (0.72 g)
5 mm ruby bead
Flow entrance

Figure 2

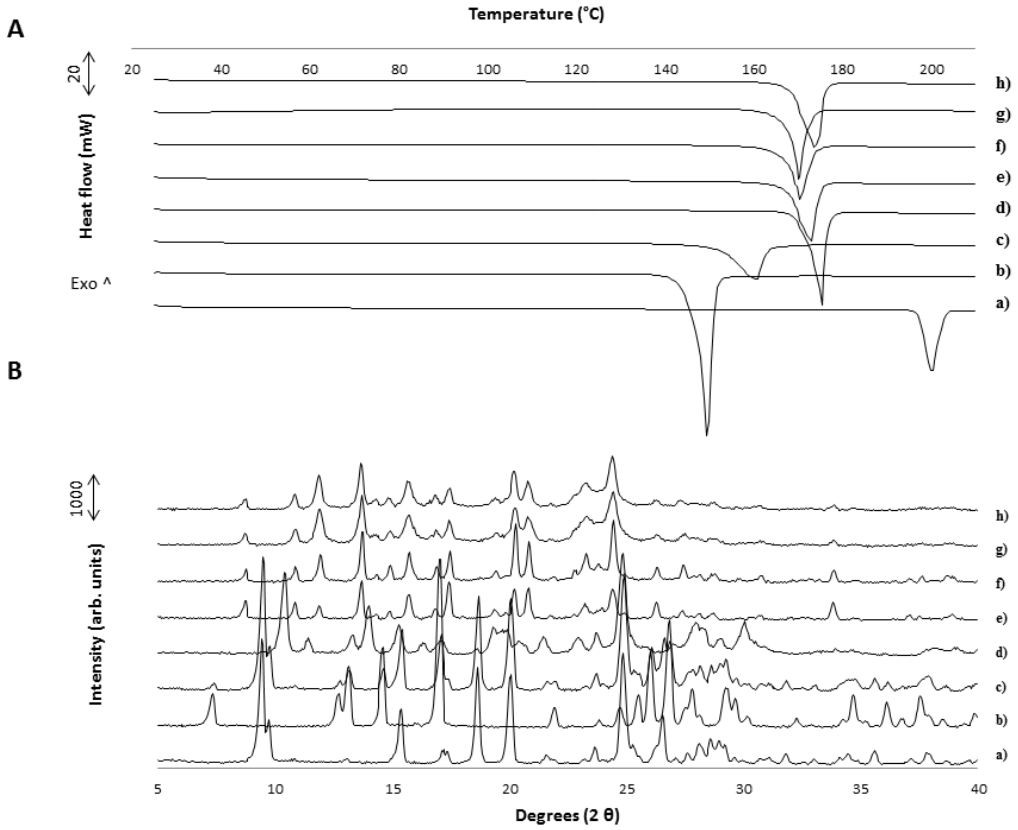
A
Temperature (°C)
20
40
60
80
100
120
140
160
180
200
20
Heat flow (mW)
Exo ^
h)
g)
f)
e)
d)
c)
b)
a)
B
1000
Intensity (arb. units)
h)
g)
f)
e)
d)
c)
b)
a)
5
10
15
20
25
30
35
40
Degrees (2 θ)

Figure 3

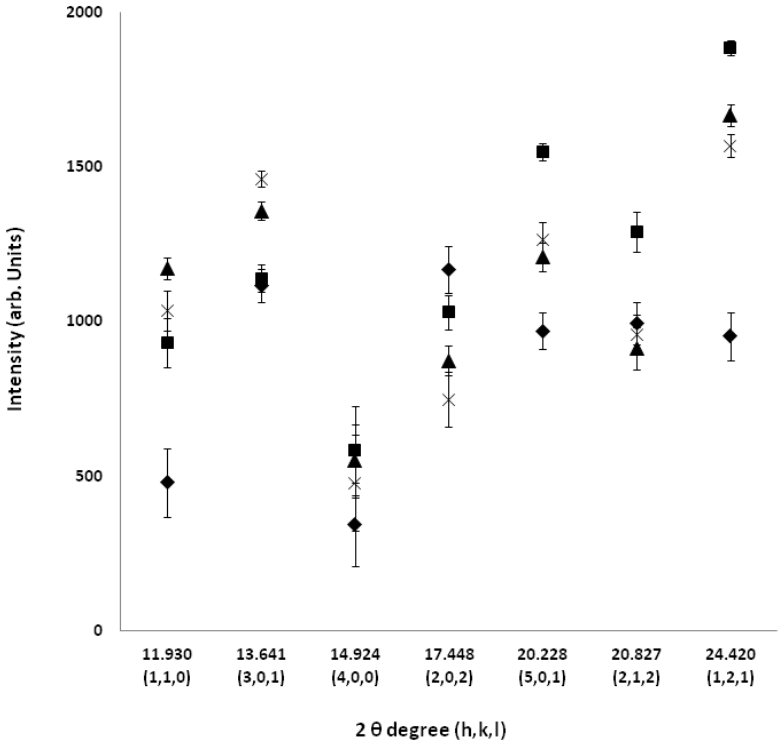
2000
1500
1000
500
0
Intensity (arb. Units)
11.930
(1,1,0)
13.641
(3,0,1)
14.924
(4,0,0)
17.448
(2,0,2)
20.228
(5,0,1)
20.827
(2,1,2)
24.420
(1,2,1)
2 θ degree (h,k,l)

Figure 4

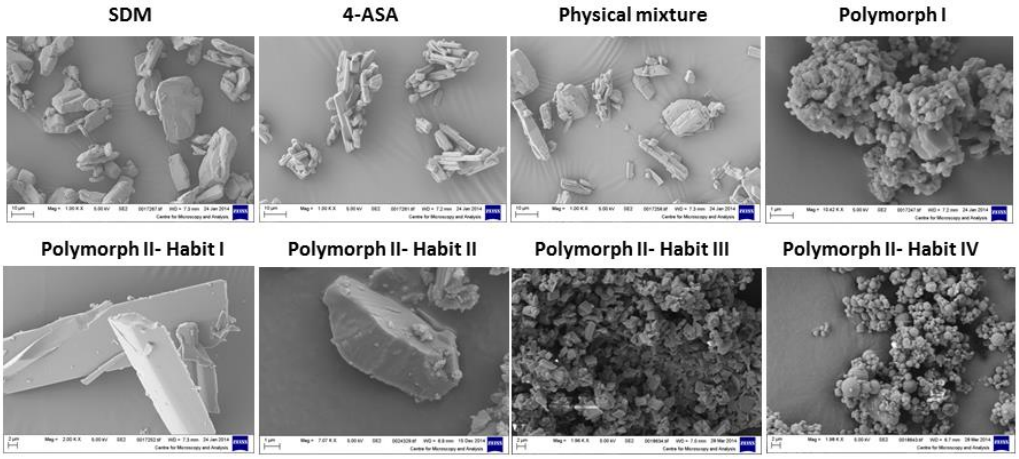
SDM
4-ASA
Physical mixture
Polymorph I
Polymorph II- Habit I
Polymorph II- Habit II
Polymorph II- Habit III
Polymorph II- Habit IV

Figure 5

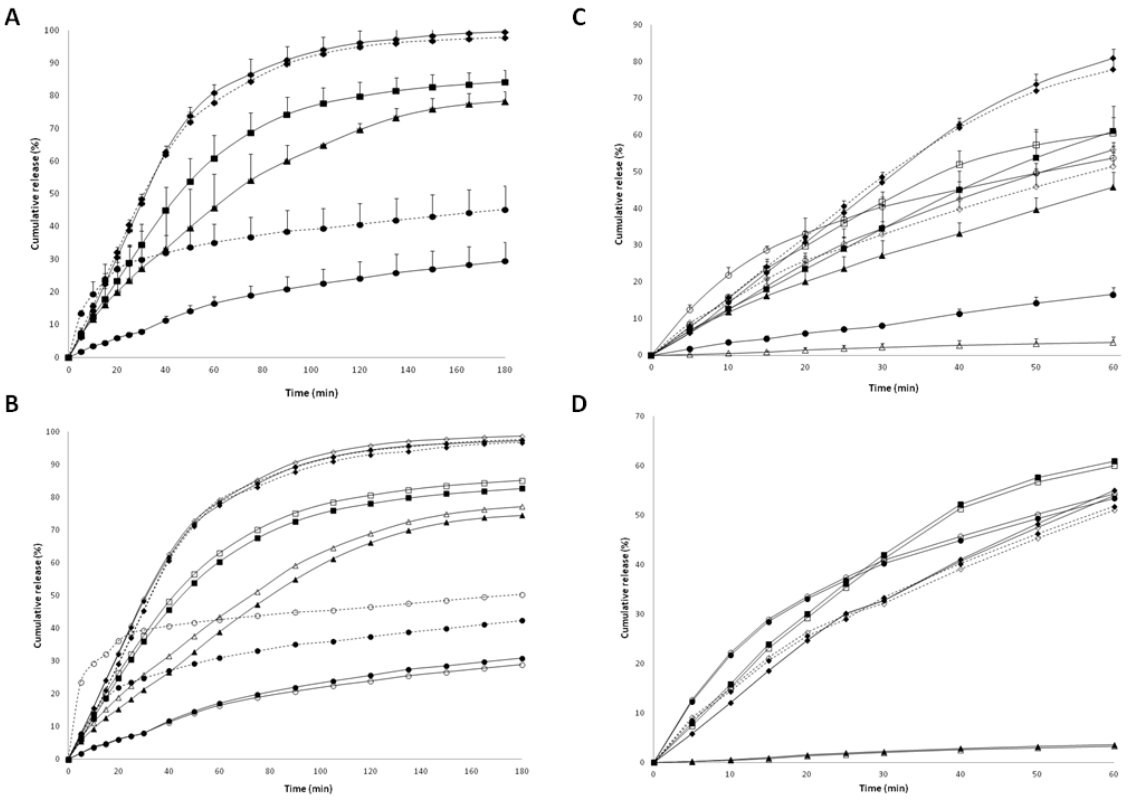
A
Cumulative release (%)
Time (min)
B
Cumulative release (%)
Time (min)
C
Cumulative relese (%)
Time (min)
D
Cumulative release (%)
Time (min)

Figure 6

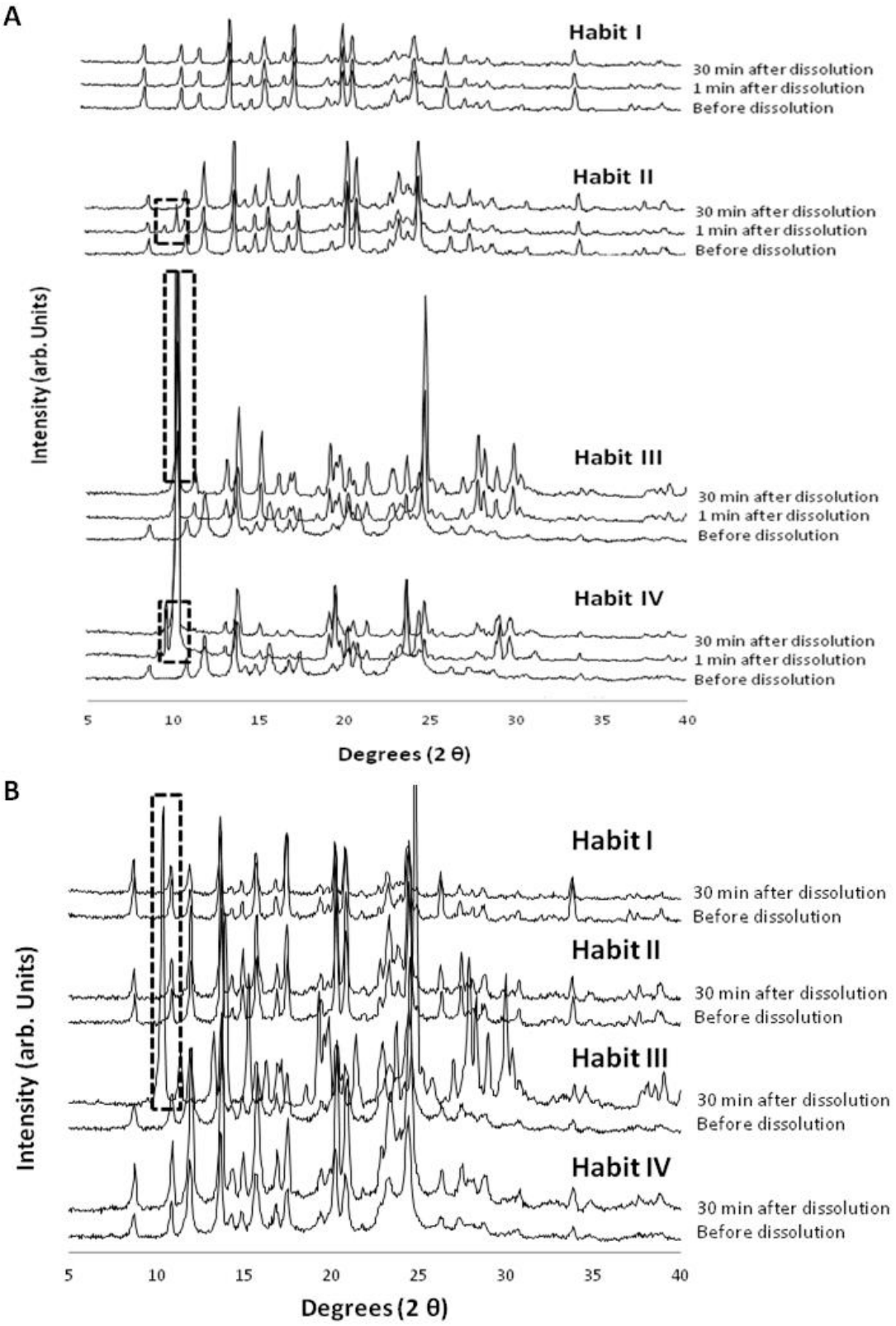
A
Habit I
30 min after dissolution
1 min after dissolution
Before dissolution
Habit II
30 min after dissolution
1 min after dissolution
Before dissolution
Habit III
30 min after dissolution
1 min after dissolution
Before dissolution
Habit IV
30 min after dissolution
1 min after dissolution
Before dissolution
Intensity (arb. Units)
5
10
15
20
25
30
35
40
Degrees (2 θ)
B
Habit I
30 min after dissolution
Before dissolution
Habit II
30 min after dissolution
Before dissolution
Habit III
30 min after dissolution
Before dissolution
Habit IV
30 min after dissolution
Before dissolution
Intensity (arb. Units)
5
10
15
20
25
30
35
40
Degrees (2 θ)

Figure 7